Optical Engineering

OpticalEngineering.SPIEDigitalLibrary.org

Mixed sensitivity H-infinity control of an adaptive optics system

Dingan Song
Xinyang Li
Zhenming Peng

SPIE.

Dingan Song, Xinyang Li, Zhenming Peng, "Mixed sensitivity H-infinity control of an adaptive optics system," *Opt. Eng.* **55**(9), 094106 (2016), doi: 10.1117/1.OE.55.9.094106.

Mixed sensitivity H-infinity control of an adaptive optics system

Dingan Song,[a,b,c,d,*] Xinyang Li,[a,c] and Zhenming Peng[b]
[a]Chinese Academy of Sciences, Key Laboratory on Adaptive Optics, Guangdian Avenue #1, Shuangliu, Chengdu, Sichuan 610209, China
[b]University of Electronic Science and Technology of China, No. 4, Section 2, North Jianshe Road, Chengdu, Sichuan 610209, China
[c]Institute of Optics and Electronics, Chinese Academy of Sciences, Guangdian Avenue #1, Shuangliu, Chengdu, Sichuan 610209, China
[d]University of Chinese Academy of Sciences, No. 19(A), Yuquan Road, Shijingshan District, Beijing 100049, China

Abstract. Design of the controller of an adaptive optical system is very complex because its model is usually with uncertainty. To deal with uncertainty and to improve robust stability, the mixed sensitivity H_∞ control has been introduced to design the controller. In order to testify the validity, wavefront aberration correction capability as well as the robust stability has been compared between the mixed sensitivity H_∞ controller and the classic integral controller. The computer simulation results demonstrate that the system with the mixed sensitivity H_∞ controller, though it cannot guarantee a better correction performance, has greater robust stability than the one with the classic integral controller. That is to say, greater robust stability is achieved at the expense of the correction capability in the system with H_∞ controller. Moreover, the greater the uncertainty is, the more proceeds the mixed sensitivity H_∞ controller will produce. It proves the efficiency of the mixed sensitivity H_∞ controller in dealing with uncertainty in adaptive optics system. [DOI: 10.1117/1.OE.55.9.094106]

Keywords: control; adaptive optics; uncertain system; wavefront aberration.

Paper 160945 received Jun. 20, 2016; accepted for publication Sep. 7, 2016; published online Sep. 28, 2016.

1 Introduction

An adaptive optics (AO) system is a complex system. Many uncertain factors exist in its model, such as time delay and gain of system. These uncertainties will reduce the performance, or even jeopardize its stability. In engineering, the stability is enhanced, more often than not, by either choosing conservative parameters for the classic integral controller or by stopping unit loops that fail to work. Due to this, the AO system stability is guaranteed at the heavy expense of its correction performance. Therefore, it is our hope to study a method that can ensure the stability of an AO system while maintaining its correction performance. Owing to its excellent capacity in tackling uncertainty, robust control was selected in our study.

Up to now, some scholars have already done research on robust control applying to AO systems. Denis et al.[1] designed the controller of an AO system with H_∞ control and carried out some analysis as well as simulation. Frazier et al.[2] adopted a multiplicative perturbation model to the modeling of the piezoelectric deformable mirror (DM) and verified the efficiency of H_∞ control on test platform. Kim et al.[3] reduced the model order by observing Hank singular values based on the observability and controllability of the plant model. Guesalaga et al.[4] added a second-order filter in weighting function of sensitivity function in the design of H_∞ controller, improving AO system antidisturbance ability at the price of the simplicity of the system. Xin and Caiwen[5,6] introduced a new method to design an AO system controller based on mixed H_2/H_∞ control, in a way that not only a smaller residual wavefront gradient tilt would be achieved, but also greater robust stability ensured. Most of those studies are emphasized on the performance of the AO system but neglected robust stability.

In this paper, to deal with the uncertainty of time delay and gain, the multiplicative perturbation model was used modeling the system and then designing the controller with H_∞ theory. Finally, the system's stability and efficiency are analyzed by computer simulation.

In Sec. 2, we describe the AO system with the multiplicative perturbation model. In Sec. 3, we design the controller with the H_∞ theory. In Sec. 4, we analyze the frequency response of the sensitivity function and complementary sensitivity function. In Sec. 5, we give a simulation about an AO system to correct the atmospheric turbulences. Finally, the conclusions are stated in Sec. 6.

2 Principium and Model of AO System

The typical AO system in chronometer observation action is shown in Fig. 1. Light rays from natural guide star occur to phase aberration after being affected by atmospheric turbulences and enter the telescope system. The rays reach the DM by reflector (M1). After correction by DM, parts of the rays are reflected to the science camera for imaging by spectroscope, and other parts reach the wavefront sensor (WFS) via the spectroscope. Then, wavefront error signals are sent to the controller to compute control signals, which will be transmitted to control the DM's work. The whole process forms a closed feedback control loop, which can eliminate aberration at real time and get a high-resolution image of the target star.

Generally, an AO system is a typical multi-input multi-output system with cross coupling. But by applying decomposition techniques, it can be an equivalent of diagonal

*Address all correspondence to: Dingan Song, E-mail: psupgpv@16X3.com

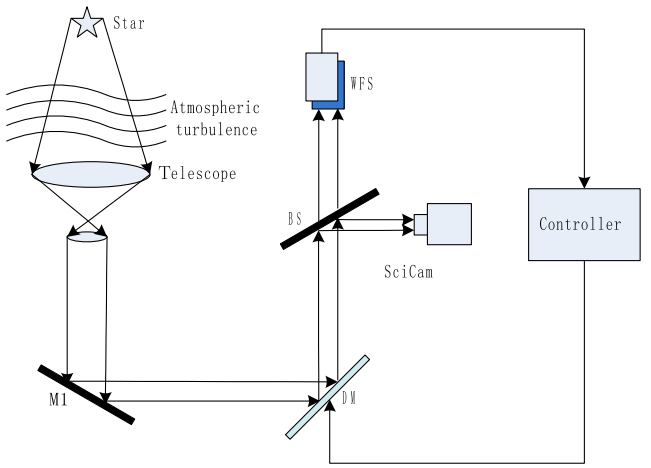

Fig. 1 Principle diagram of AO system.

system. Once uncoupled, a single-input single-output controller can be applied to the uncoupled channels. Figure 2(a) shows signal flow diagram of the AO system including the WFS, time delay, controller, zero order holders (ZOH), and an actuator that contains high-voltage amplifier and DM. Figure 2(b) shows a simplified diagram of the AO system from the control sight, of which the WFS, time delay, ZOH, and actuator are included in the plant $P(s)$. r is the aberration perturbation of the system, n is the detector noise, e is the wavefront error signal after correction, and y is the compensate signal. Here, the continuous domain discretization method is adopted to design the controller.

In Fig. 2(b), the plant can be depicted as follows:

$$P(s) = C(s) \cdot D(s) \cdot L(s) \cdot W_F(s), \tag{1}$$

where $C(s)$ is the transfer function of actuator, $D(s)$ is the transfer function of ZOH, $L(s)$ denotes the time delay, and $W_F(s)$ is the transfer function of WFS. The plant model $P(s)$ can be approximated to an inertia element in series with the time-delay element, i.e.,

$$P(s) = \frac{k}{T_1 s + 1} e^{-\tau s}, \tag{2}$$

where k, T_1, τ are the coefficients of gain, inertia, and time delay, respectively. According to multiplicative perturbation modeling method, $P(s)$ can be separated into the linear part and the nonlinear part. It is depicted as follows:

$$P(s) = P_m(s)[1 + W_\Delta(s) \cdot \Delta(s)], \tag{3}$$

where $P_m(s)$ denotes the nominal model description of the physical system, $W_\Delta(s) \cdot \Delta(s)$ denotes the unmodeled dynamics, and $W_\Delta(s)$ denotes the weight function of the unmodeled dynamics, $\|\Delta(s)\|_\infty \le 1$. $W_\Delta(s)$ must be satisfied the inequality as follows:

$$|W_\Delta(s)| > \left| \frac{P(s) - P_m(s)}{P_m(s)} \right|. \tag{4}$$

Gain coefficient, inertia coefficient, and time-delay coefficient can be achieved via identifying measurements provided by a scanning vibrometer. Here, the inertia coefficient T_1 is equal to $1/680$, the gain coefficient k ranges from 0.7 to 1.3, and the time-delay coefficient τ is uncertain within 1 ms $\le \tau \le$ 2 ms. Nine models of $P(s)$ under different states are built up by choosing $k = (0.7, 1, 1.3)$ and $\tau = (1, 1.5, 2)$ ms, shown in Table 1.

The nominal model can be got by Pade approximation of P_{22}, i.e.,

$$P_m(s) = \frac{-1.3\ \mathrm{s} + 1333}{0.001471 s^2 + 2.961 s + 1333}. \tag{5}$$

Table 1 Nine models under the different value of gain k and time delay τ.

	k		
τ (ms)	0.7	1	1.3
1	P_{11}	P_{12}	P_{13}
1.5	P_{21}	P_{22}	P_{23}
2	P_{31}	P_{32}	P_{33}

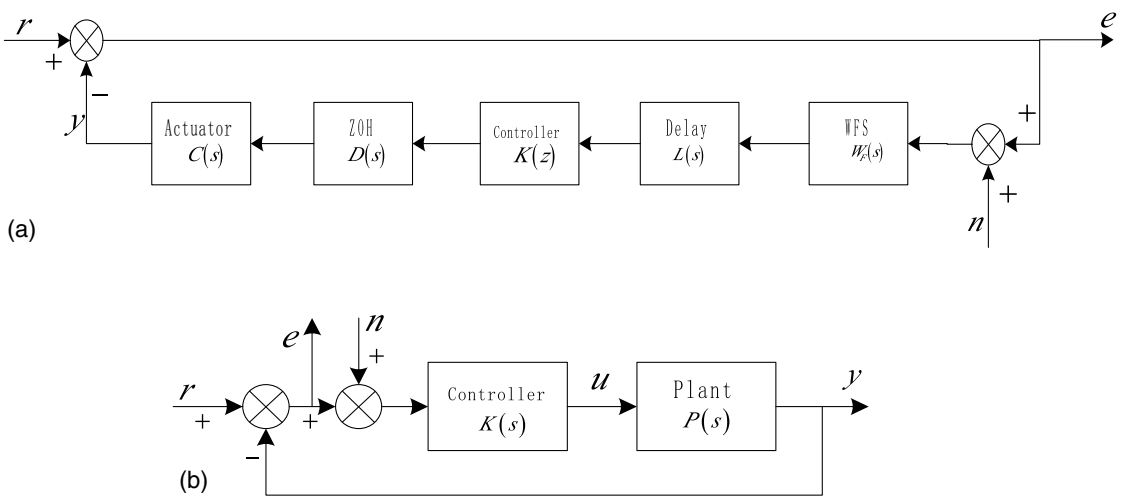

Fig. 2 Diagram block of AO system (a) detailed structure and (b) simplify structure.

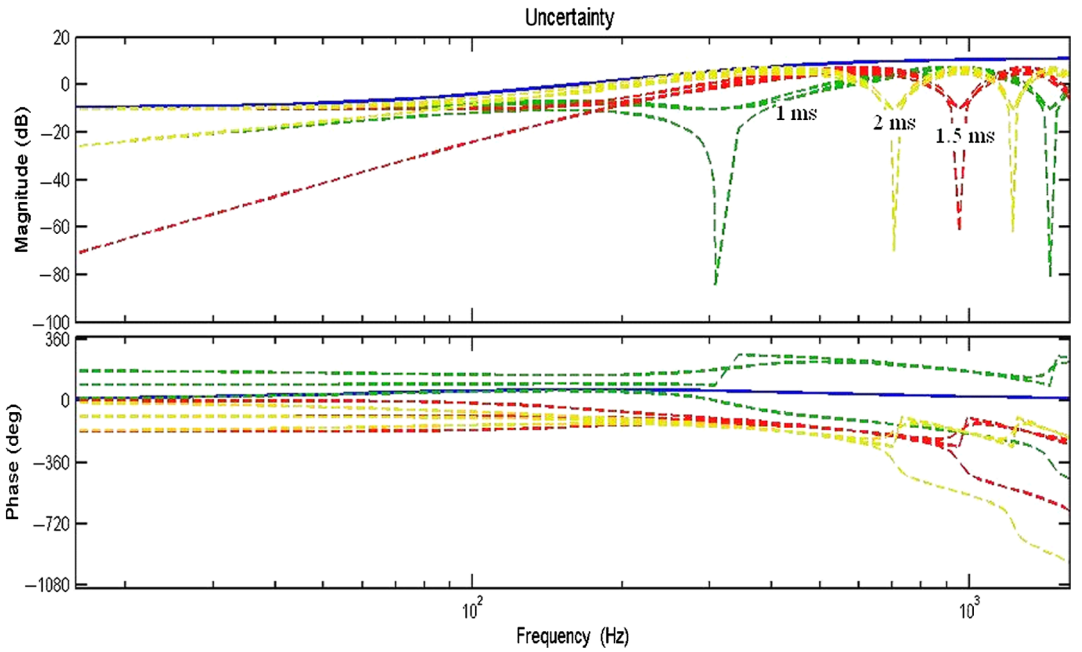

Fig. 3 Bode plot of the uncertainty (dashed line) and weighting function (solid line).

From inequality (4), the weighting function of uncertainty can be chosen in Eq. (6). The bode plot of the uncertainty and weighting function are shown in Fig. 3 by dashed line and solid line, respectively

$$W_\Delta(s) = \frac{9.167e-07s^2 + 0.0011s + 0.33}{2.5e-07s^2 + 0.001s + 1}. \tag{6}$$

3 Controller Design

The standard H_∞ configuration is shown in Fig. 4. The external inputs are denoted by r. q denotes the evaluating signals to be minimized/penalized that include both performance and robustness measures, y is the vector of measurements available to the controller, $K(s)$ and u are the vectors of control signals. $M(s)$ is called generalized plant or interconnected system. The objective is to find a stabilized controller $K(s)$ to guarantee internal stability of the closed-loop system and at the meantime, to ensure that the H_∞ norm of the closed-loop transfer function from r to q is less than a given positive number, i.e.,

$$\|F_l(M,K)\|_\infty < \eta, \tag{7}$$

where $F_l(M,K)$ is the closed-loop transfer function from r to q, and η is a constant. Usually, the robust index can be defined as γ by the following equation:

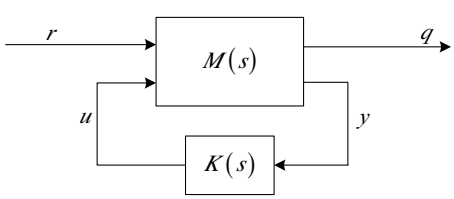

Fig. 4 Standard H_∞ configuration.

$$\gamma = \|F_l(M,K)W_\Delta(s)\|_\infty. \tag{8}$$

From Fig. 2, the open-loop transfer function is

$$G(s) = K(s)P(s). \tag{9}$$

Define the sensitivity function, control sensitivity function, and complementary sensitivity function by Eqs. (10)–(12), so the control sensitivity function is equal to the closed-loop transfer function:

$$\text{sensitivity function: } S(s) = \frac{e(s)}{r(s)} = \frac{1}{1+G(s)}, \tag{10}$$

$$\text{control sensitivity function: } T(s) = \frac{y(s)}{r(s)} = \frac{G(s)}{1+G(s)}, \tag{11}$$

$$\text{complementary sensitivity function: } K(s)S(s) = \frac{u(s)}{r(s)} = \frac{K}{1+G}. \tag{12}$$

Then, the error signal e and control signal u can be obtained easily from Fig. 2

$$e(s) = \frac{1}{1+G}r - \frac{G}{1+G}n = S(s)r(s) + T(s)n(s). \tag{13}$$

$$u(s) = \frac{K}{1+G}r + \frac{K}{1+G}n = K(s)S(s)[r(s) + n(s)]. \tag{14}$$

From Eqs. (13) and (14), limiting the magnitude of $\|S(s)\|_\infty$ and $\|T(s)\|_\infty$ can reduce the influence from both

external aberration perturbation and detector noise over error signals. According to the small gain theorem, the smaller $\|T(s)\|_\infty$ is, the better the system robust stability will be. Furthermore, energy consumed output control signals can be reduced by restricting the magnitude of $\|K(s)S(s)\|_\infty$, thus improving engineering efficiency. Therefore, it is usually the practice to limit simultaneously the magnitude of $\|S(s)\|_\infty$, $\|T(s)\|_\infty$, and $\|K(s)S(s)\|_\infty$ in engineering.

The block diagram of H_∞ control of the AO system is shown in Fig. 5, in which the broken line contain the generalized plant $M(s)$. It is easy to know that

$$\begin{bmatrix} q \\ y \end{bmatrix} = M(s)\begin{bmatrix} r \\ u \end{bmatrix} = \begin{bmatrix} M_{11}(s) & M_{12}(s) \\ M_{21}(s) & M_{22}(s) \end{bmatrix}\begin{bmatrix} r \\ u \end{bmatrix} = \begin{bmatrix} W_1(s)\times 1 & -W_1(s)\times P_m(s) \\ 0 & W_2(s) \\ 0 & W_3(s)\times P_m(s) \\ 1 & -P_m(s) \end{bmatrix}\begin{bmatrix} r \\ u \end{bmatrix}, \tag{15}$$

$$u(s) = K(s)y(s), \tag{16}$$

where $z = [\,z_1 \quad z_2 \quad z_3\,]^{\mathrm{T}}$, the superscript T means matrix transpose and the evaluating signals

$$q(s) = \begin{bmatrix} q_1(s) \\ q_2(s) \\ q_3(s) \end{bmatrix} = \begin{bmatrix} W_1(s)e(s) \\ W_2(s)u(s) \\ W_3(s)y(s) \end{bmatrix} = \begin{bmatrix} W_1(s)S(s) \\ W_2(s)K(s)S(s) \\ W_3(s)T(s) \end{bmatrix} r(s). \tag{17}$$

Define $Q(s)$ as

$$Q(s) = \begin{bmatrix} Q_1(s) \\ Q_2(s) \\ Q_3(s) \end{bmatrix} = \begin{bmatrix} W_1(s)S(s) \\ W_2(s)K(s)S(s) \\ W_3(s)T(s) \end{bmatrix}. \tag{18}$$

Then according to Eq. (7), the objective of H_∞ control is to find a stabilized controller $K(s)$ to make the closed-loop system internally stable and, in the meantime, to ensure that the H_∞ norm of $Q(s)$ is less than a given positive number. That is to say

$$\|Q(s)\|_\infty < \eta. \tag{19}$$

Based on the generalized plant $M(s)$, the controller can be solved by the robust control toolbox of MATLAB.[7] The weighting function $W_1(s)$ is a low-pass filter to shape the sensitivity function $S(s)$. Then, $S(s)$ is a high-pass filter that can minimize the error signals e. The weighting function $W_2(s)$ is a high-pass filter with a crossover frequency that approximately equals to the desired closed-loop bandwidth. It contributes to the robustness of the closed-loop system by minimizing the controller output. The weighting function $W_3(s)$ is a high-pass filter to shape the complementary sensitivity function $CS(s)$. So, $CS(s)$ is a low-pass filter that can restrain the high-frequency element of noise. An excellent controller can be designed by choosing the suitable weighting functions.

4 Performance of Controller

4.1 *Integrator*

The integrator controller is the simplest and the most common controller in an AO system. It is defined by

$$K(z) = \frac{g}{1 - az^{-1}}, \tag{20}$$

where z is the Z-transform operator and a is the generally unity, unless a controller free from winding-up is desired. Parameter g represents the gain of the loop and is adjusted according to noise and performance requirements. An optimal way to define this gain is proposed by Gendron and Lene.[8] Figure 6 shows the curve of Rms(err)/Rms(open) with the variance of g, where Rms(err) means the RMS (root mean square) of error signals of integrator control system, and Rms(open) means the RMS (root mean square) of output signals of open-loop system. The trend of the value of Rms(err)/Rms(open) is minus at first but gradually becomes bigger after the optimal value of g. Here, when $g = 0.305$, $a = 1$, the system obtains the best performance. The robust index $\gamma_i = 0.4337$. Phase margins of nine different states are shown in Table 2. The phase margins decreases with the increase of the k or τ, respectively.

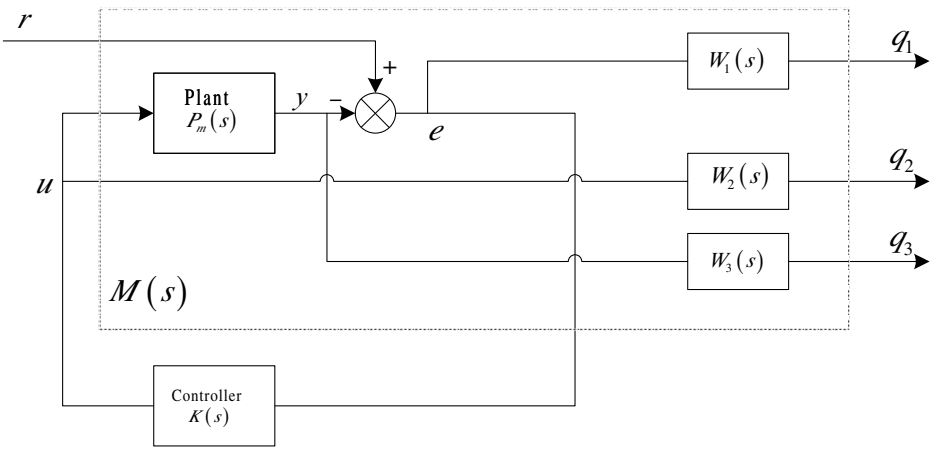

Fig. 5 Block diagram of generalized plant the H_∞ controller.

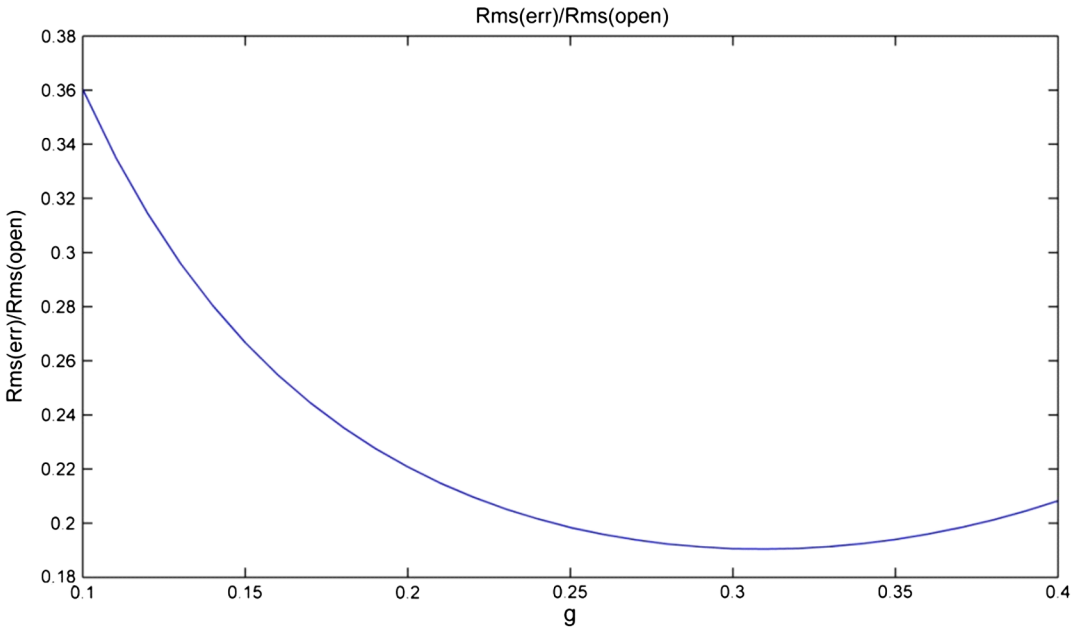

Fig. 6 The curve of Rms(err)/Rms(open).

Table 2 Phase margins of nine different states with integrator.

	k		
τ (ms)	0.7	1	1.3
1	72.7841	66.3113	60.4660
1.5	66.8107	57.9473	49.8313
2	60.8374	49.5833	39.1967

Table 3 Phase margins of nine different states with H_∞ controller.

	k		
τ (ms)	0.7	1	1.3
1	88.16	83.7327	79.7896
1.5	83.8143	77.4607	71.5342
2	79.4687	71.1886	63.2788

4.2 H_∞ Control

From the former chapter, the weight functions of sensitivity function, control sensitivity function, and complementary sensitivity function can be chosen, respectively, as follows:

$$W_1(s) = \frac{110}{0.08s + 1}, \tag{21}$$

$$W_2(s) = 0.5 \times \frac{10^{-2}s + 1}{10^{-4}s + 1}, \tag{22}$$

$$W_3(s) = 2 \times \frac{10^{-2}s + 1}{10^{-3}s + 1}. \tag{23}$$

Then, the controller can be solved as follows by the function mixsyn in the MATLAB robust control toolbox

$$K(s) = \frac{9685.8(s + 1e04)(s + 1333)(s + 1000)(s + 680)}{(s + 7.639e04)(s + 1108)(s + 12.5)(s^2 + 3281s + 4.81e06)}. \tag{24}$$

And the discrete controller

$$K(z) = \frac{0.63962(z - 0.5975)(z - 0.3376)(z^2 - 0.1746z + 0.01066)}{z(z - 0.9876)(z - 0.3302)(z^2 - 0.04457z + 0.03759)}. \tag{25}$$

With the necessary weights selected above, the control design algorithm provides a controller with a H_∞ performance index $\gamma_{ro} = 0.3879 < \gamma_i = 0.4337$. Therefore, the system with H_∞ controller has a better robustness than the system with integrator. The phase margins of nine different states with the H_∞ controller are shown in Table 3. It is easy to know that a large phase margin can be obtained by using H_∞ control. From Table 4, it is easy to know that the phase margin can be increased by 15.3759 to 24.0821.

According to Eqs. (13) and (14), error signals are determined by the character of sensitivity function and complementary sensitivity function. The bode plots of $S(s)$ and

Table 4 The increase of phase margins of nine different states.

	k		
τ (ms)	0.7	1	1.3
1	15.3759	17.4214	19.3236
1.5	17.0036	19.5133	21.7028
2	18.6313	21.6052	24.0821

$T(s)$ are shown in Figs. 7 and 8, where the solid line represents the system with H_∞ controller and the dashed line shows the system with integrator. Two conclusions can be made from Fig. 7. First, the bandwidths of the sensitivity function provided by the two methods are almost the same. However, the integrator is better than the H_∞ controller in error mitigation at the low frequency. Second, the overshoot of the sensitivity function provided by the H_∞ controller is smaller than that provided by the integrator, which is because H_∞ control limits the power of control

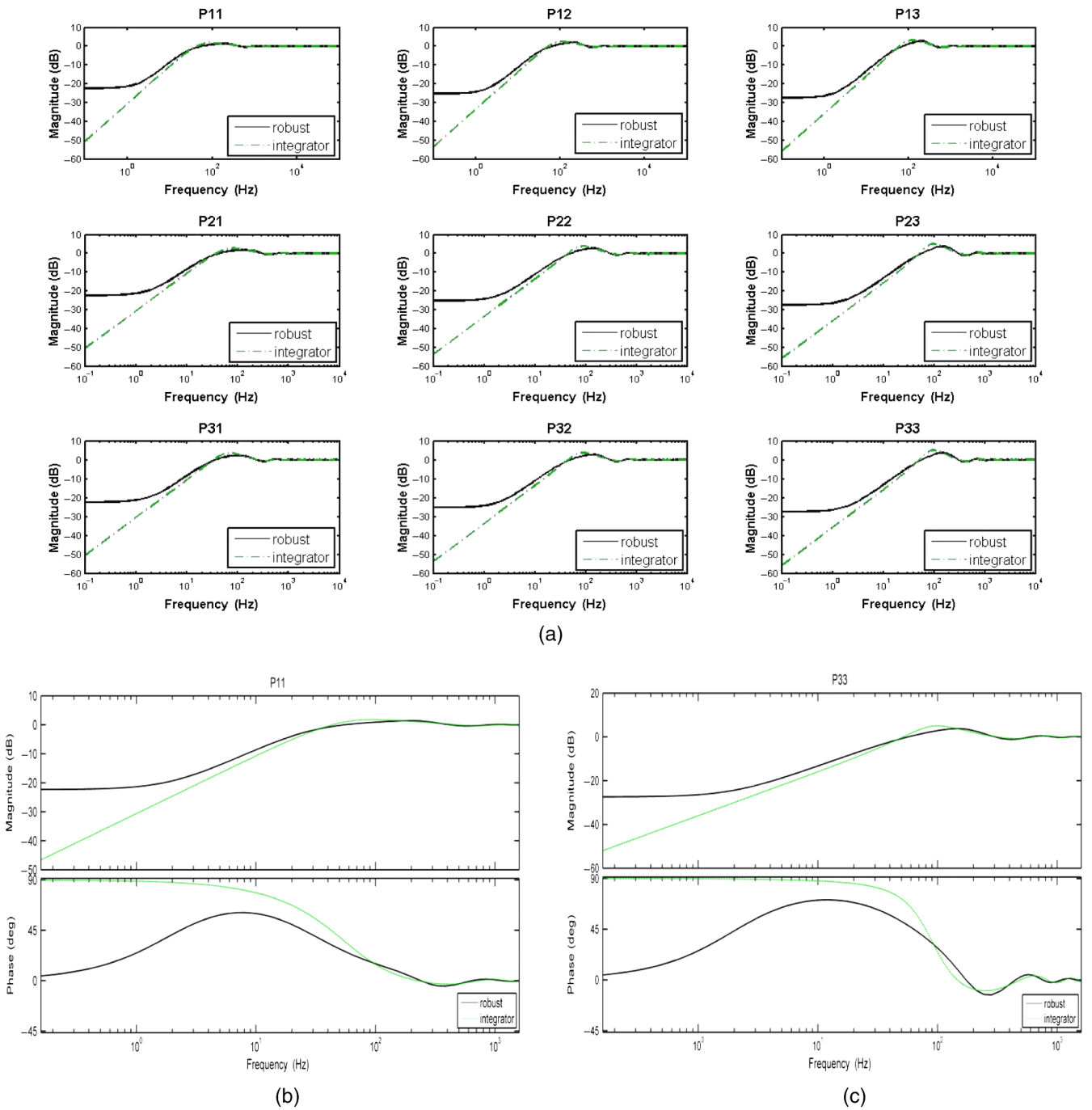

Fig. 7 The bode plot of sensitivity function: (a) nine magnitude figures of different states; (b) the bode plot of P11 state. It includes the phase versus Hz figure; and (c) the bode plot of P33 state with the phase versus Hz figure.

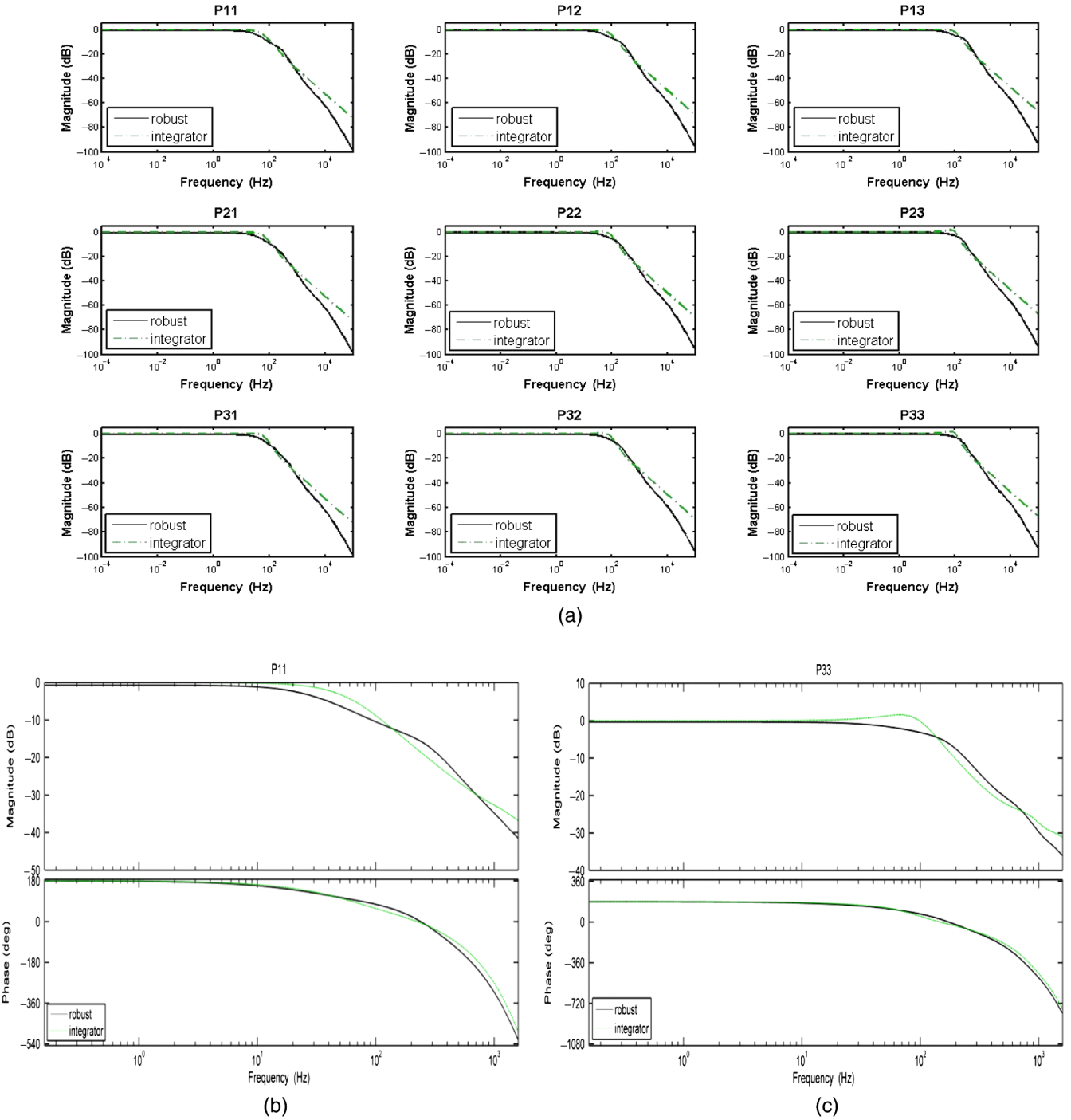

Fig. 8 The bode plot of complementary sensitivity function: (a) nine magnitude figures of different states; (b) the bode plot of P11 state. It includes the phase vesus Hz figure; and (c) the bode plot of P33 state with the phase versus Hz figure.

signals. Figure 8 shows that the two methods have almost the same bandwidth; nevertheless, the system with the H_∞ controller has greater capability in restraining the noise.

5 Simulation Results

From Ref. 9, the characteristic parameters of Fred constant r_0 and Greenwood frequency F_g can be calculated by the power spectral density (PSD) of atmospheric turbulence. Consequently, time series of atmospheric turbulence can be inversed. From Ref. 10, the detector noise can be supposed as gauss white noise. Here, the sampling period of an AO system is 1 ms, D/r_0 is 26.79, Greenwood frequency is 130 Hz, and the signal-to-noise ratio is 6.

The PSDs of error signals of computer simulation are shown in Fig. 9, where the dot-dashed lines are the output of the open-loop system, the solid lines are the error signals of the system with H_∞ controller, and the dashed lines are the error signals of the system with integrator. Two conclusions can be made from Fig. 9: one is that error suppression

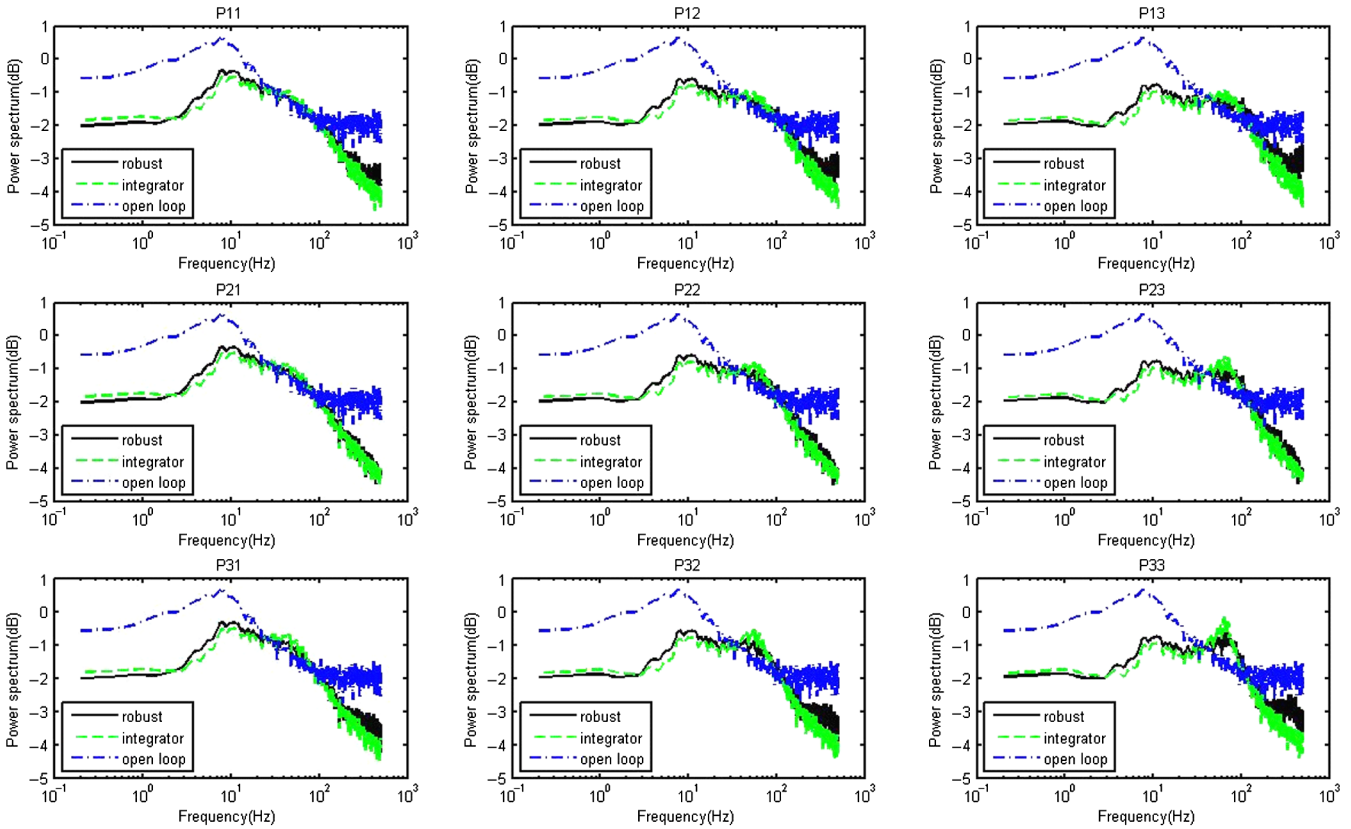

Fig. 9 The PSDs of error signals.

Table 5 Statistical simulation result of AO system.

	De/Dopen	De1/Dopen	De1/De	De	De1	Dopen	epv	e1pv	openpv
P11	0.2165	0.1930	0.8914	8.5796	7.6478	39.6244	12.2081	11.1820	27.8891
P12	0.1766	0.1617	0.9153	6.9982	6.4056	39.6244	11.0360	9.9713	27.8891
P13	0.1719	0.1591	0.9257	6.8096	6.3039	39.6244	10.7476	9.3977	27.8891
P21	0.2323	0.2176	0.9366	9.2043	8.6207	39.6244	12.6130	11.6171	27.8891
P22	0.1934	0.1942	1.0042	7.6643	7.6964	39.6244	11.5189	10.6707	27.8891
P23	0.1928	0.2101	1.0897	7.6408	8.3265	39.6244	10.8675	10.9449	27.8891
P31	0.2561	0.2519	0.9839	10.1465	9.9829	39.6244	12.9506	12.0457	27.8891
P32	0.2282	0.2518	1.1037	9.0412	9.9786	39.6244	11.9634	11.6993	27.8891
P33	0.2545	0.3395	1.3340	10.0843	13.4523	39.6244	12.2049	12.4200	27.8891
	Ee	Ee1	Eopen	upv	u1pv	Eu	Eu1	Du	Du1
P11	−0.0064	−0.0096	0.0359	31.7525	34.1556	0.0459	0.0506	56.8279	71.4228
P12	−0.0078	−0.0101	0.0359	24.4461	25.2931	0.0335	0.0359	32.6988	37.7232
P13	−0.0085	−0.0105	0.0359	20.3650	20.2927	0.0264	0.0278	21.9137	23.6816
P21	−0.0064	−0.0096	0.0359	32.0992	34.4634	0.0462	0.0509	58.4940	74.2201
P22	−0.0078	−0.0100	0.0359	24.6833	25.6156	0.0337	0.0361	33.8149	39.7076
P23	−0.0086	−0.0105	0.0359	20.4228	20.3069	0.0265	0.0281	22.8448	25.5831
P31	−0.0063	−0.0096	0.0359	32.4298	34.7782	0.0464	0.0511	60.3599	77.4899
P32	−0.0077	−0.0098	0.0359	24.9338	26.1448	0.0339	0.0363	35.2826	42.5109
P33	−0.0087	−0.0100	0.0359	20.5205	19.7367	0.0268	0.0287	24.4982	29.4496

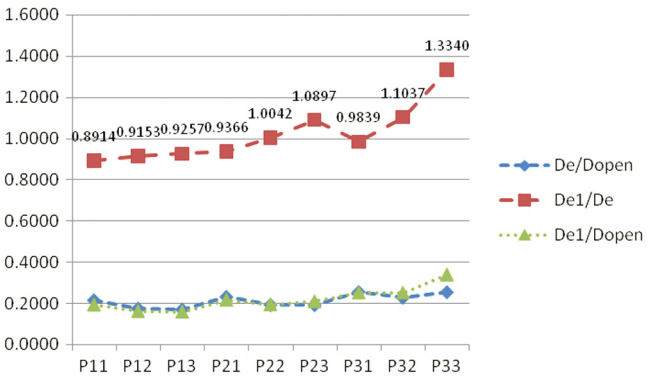

Fig. 10 Line chart of corrected rate of AO system.

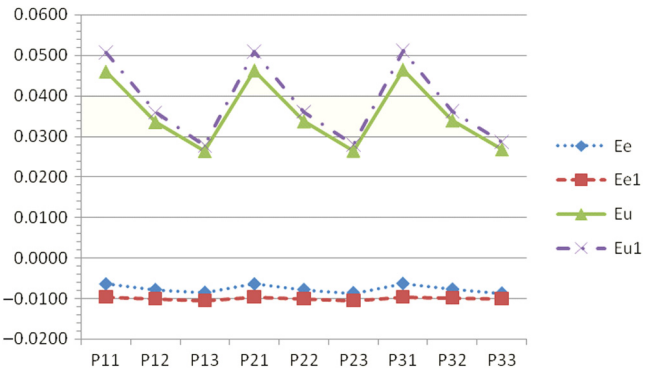

Fig. 12 Line chart of mean value of control signal and error signal.

bandwidths of two methods equal approximately, for their restraining bandwidths of sensitivity functions are the same. The other one is that the system with H_∞ controller is better than the one with integrator in restraining error signal at middle frequency instead of low frequency. The two methods have the same capability in restraining noise at high frequency, and they both have peak values at middle frequency. However, the peak value of the former is smaller.

Table 5 and Figs. 10–13 show detailed statistical results of the simulation. In Table 5, $P_{11} \sim P_{33}$ denote nine models of different states; De, De1, and Dopen denote the variance of error signals with the H_∞ control, integrator, and open-loop system, respectively; De/Dopen denotes the ratio of the variance of error signals with the H_∞ control to the variance of open-loop error signals, De1/Dopen denotes the ratio of the variance of error signals with the integrator to the variance of open-loop error signals. The smaller the ratio value is, the better the controller performance will be. De1/De denotes the variance ratio of the closed-loop error signal of AO system with integrator and the one with H_∞ controller. It shows the comparison between the integrator and H_∞ control in terms of correction capability. upv and u1pv denote the peak value of control signals of H_∞ controller and integrator, respectively. epv and e1pv denote the peak value of mean value of error signal of H_∞ controller and integrator, respectively. Ee, Ee1, and Eopen denote the mean value of error signal of H_∞ controller, integrator, and open-loop errors, respectively. Eu and Eu1 denote the mean value of control signal of H_∞ controller and integrator, respectively. Du and Du1 denote the variance of control signal of H_∞ controller and integrator, respectively.

Figure 10 and Table 5 show that both time delay and gain can exert negative influence on the performance of AO system. With the gain increasing, the proceeds of the H_∞ controller will be reduced. In contrast, the increase of time delay will enhance the benefits to the H_∞ controller. It also demonstrates that the integrator is more suitable in designing a controller when time delay is small. Figure 11 shows the line chart of variance and peak value of control signal. The variance charts show that the control signals of the integrator varies more dramatically than that of the H_∞ controller. This makes the later more powerful in resisting the effect of uncertainty. Variance value will be reduced with the increase of the gain and increased with the increase of the delay. That is to say, the delay has a positive influence on the control signal, whereas the gain has a negative influence. The peak value charts show that the two methods are almost the same. This is because in some extreme instances big control signals are needed to drive the DM. Figure 12 shows the line chart of the mean value of error signal and control signal. Figure 13 shows the line chart of the error signals' variance value and peak value. Figure 12 proves that the H_∞ control is better than the integrator in terms of the mean value, because the mean value of the former is smaller than that of the later. However, from Fig. 9 and 13, a conclusion can be drawn that the H_∞ control, while strong at guaranteeing the stability of the system, cannot ensure a better performance of the system, for it costs the performance to improve the stability of the system.

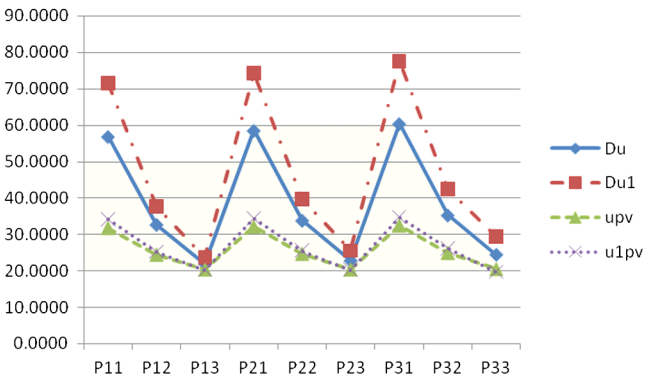

Fig. 11 Line chart of variance and peak value of control signal.

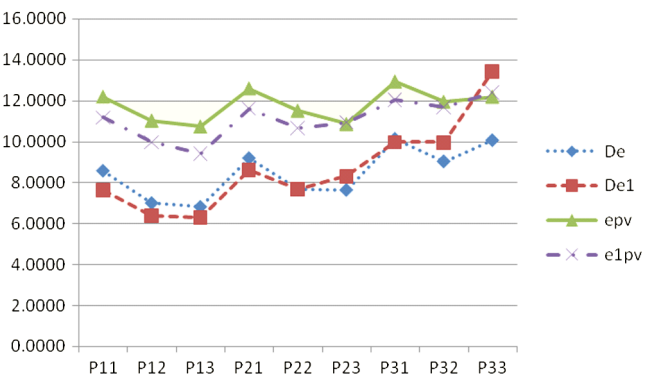

Fig. 13 Line chart of variance value and peak value of error signal.

6 Conclusion

In this paper, a mixed sensitivity H_∞ robust control design of the AO system is presented. Compared with the integrator, the mixed sensitivity H_∞ robust control can get a better robustness from the bode plot of sensitivity function and complementary sensitivity function. However, the results of the simulation also show that a better performance cannot always be guaranteed by employing the mixed sensitivity H_∞ robust control. In some cases, the integrator has greater correction capability. The results also show that the mixed sensitivity H_∞ robust control has more advantages in AO system with a large time-delay uncertainty.

Acknowledgments

This work was supported by the National Natural Science Foundation of China, managed by the Key Laboratory on Adaptive Optics, Chinese Academy of Sciences at Chengdu, Sichuan under Grant No. 61205069.

References

1. N. Dens et al., "H_∞ control design for an adaptive optics system," *Kybernetika* **35**(1), 69–81 (1999).
2. B. W. Frazier et al., "Theory and operation of a robust controller for a compact adaptive optics system," *Opt. Eng.* **43**(12), 2912–2920 (2004).
3. J. H. Kim, D. C. Burtz, and B. N. Agrawal, "Wavefront correction of optical beam for large space mirrors using robust control techniques," *Acta Astronaut.* **68**, 141–148 (2011).
4. A. Guesalaga et al., "Comparison of vibration mitigation controllers for adaptive optics systems," *Appl. Opt.* **51**(19), 4520–4535 (2012).
5. Z. Xin and M. A. Caiwen, "Research on nonsmooth H_∞ control for the adaptive optics system," *Acta Photonica Sin.* **43**(9), 1–5 (2014).
6. Z. Xin and M. Caiwen, "Design and simulation of the adaptive optics system based on mixed H_2/H_∞ control," *Acta Photonica Sin.* **43**(12), 1201003 (2014).
7. G. Balas et al., Eds., *Robust Control Toolbox 4.2.*, MathWorks, Inc., Natick (2012).
8. E. Gendron and P. Lena, "Astronomical adaptive optics I. Modal control optimization," *Astron. Astrophys.* **291**(1), 337–347 (1994).
9. G. Youming, M. A. Xiaoyu, and R. Changhui, "Modified effective bandwidths of adaptive optical control systems for compensation in Kolmogorov turbulence," *Acta Physica Sin.* **62**(13), 134207 (2013).
10. J. Wenhan, X. Hao, and S. Feng, "Detectiong error of Shack-Hartmann wavefront sensor," *Proc. SPIE* **3126**, 534–544 (1997).

Dingan Song received his BS degree in automation from the Hunan Institute of Science and Technology in 2011 and his MS degree in control theory and control engineering from the University of Northeast in 2014. He is pursuing the doctoral degree in information science and information processing at the University of Electronic Science and Technology of China. His current research interests include adaptive optics, robust control, and wavefront correction.

Xinyang li is a professor and doctoral tutor of the Chinese Academy of Sciences, Key Laboratory on Adaptive Optics. His research is focused on the signal processing and control technology of adaptive optical system, including wavefront detection technology and image restoration algorithm, high-speed wavefront signal processing and control algorithm, and the application of adaptive optics in laser atmospheric transmission, high resolution imaging, laser communication, and laser coherent synthesis, etc.

Zhengming Peng is a professor and doctoral tutor of the University of Electronic Science and Technology of China, a member of IEEE, and a member of the China Society of Astronautics. His research is focused on digital image and video signal processing, including computer vision and pattern recognition, SAR image and target recognition, photoelectric imaging target detection, recognition and tracking, earth wave imaging anomalous and complex oil and gas reservoir prediction methods, etc.